npj | climate and atmospheric science

Article

Published in partnership with CECCR at King Abdulaziz University

https://doi.org/10.1038/s41612-025-01031-x

Storylines reveal contrasting thermodynamic effects of climate change on 2020/21 East Asian cold extremes

Wenqin Zhuo[1,2,3] ✉, Antonio Sánchez-Benítez[3], Marylou Athanase[3], Thomas Jung[3,4], Yao Yao[5] ✉ & Helge F. Goessling[3]

The changing character of mid-latitude cold air outbreaks in a warming climate remains unclear, primarily due to uncertainty associated with changing atmospheric dynamics. Here, we employ an event-based storyline approach in which the evolution of the large-scale atmospheric circulation is nudged to reanalysis data at different global warming levels based on historical and medium-to-high-emission scenario simulations. We thereby quantify the thermodynamic climate-change effects of pre-industrial, 2 °C and 4 °C warmer climates compared to present-day climate for three cold surges in East Asia during winter 2020/21. The strongest warming occurs over northeast Asia, reaching up to +12 °C in a + 4 °C warmer climate and caused by the advection of less cold air from winter ice-free regions in the Arctic, where surface air temperature increases by over +20 °C. In contrast, over southern China, a moderate cooling is found from pre-industrial to present-day climates, due to the observed increase in aerosol concentration, peaking by the mid-21st century and altering radiative balances. This cooling effect is likely to persist well into a + 2 °C-warmer climate; however, it may become undetectable at the end of the 21st century (+4 °C warming). Our findings underscore the important thermodynamic impact associated with Arctic amplification and cooling effect of aerosol-induced changes in the radiation budget under a high aerosol emission scenario on East Asian cold extremes.

How will climate change impact winter extreme weather? This question is of considerable scientific and public interest. In recent decades, despite ongoing global warming and accelerated Arctic warming, i.e., Arctic amplification[1,2], mid-latitude continents continue to experience frequent cold extremes in winter[3–5]. This inevitably leads us to wonder if and how cold extremes have already been influenced by climate change and how they would unfold in a warmer future climate.

The event-based storyline approach provides a framework to measure the effects of climate change on extreme weather[6]. A well-established type of event-based storylines is the pseudo-global warming (PGW)[7,8] method based on regional climate models. In the PGW approach, typically, factual simulations are generated using initial and boundary conditions from reanalysis data, while counterfactual storylines are generated by adding perturbations (deltas) to the initial and boundary conditions. The deltas are supposed to capture how climate change would affect these conditions. The deltas can be highly idealised, e.g., using a uniform temperature perturbation and assuming that relative humidity remains unchanged, or more sophisticated, e.g., 3-dimensionally resolved fields of perturbations for temperature, humidity, and possibly more variables, derived from CMIP (Coupled Model Intercomparison Project) type climate model data[7–9]. However, in either case, these deltas are not sensitive to the exact atmospheric circulation and meteorological conditions characterising a simulated event, although such sensitivities can be substantial[10,11]. In contrast to PGW, storyline simulations based on global climate models that nudge only the large-scale winds from reanalysis data in different background climate conditions overcome this limitation. They make it possible to estimate a thermodynamical "climate change signal of the day" given a specific

[1]Yunnan Key Laboratory of Meteorological Disasters and Climate Resources in the Greater Mekong Subregion, Yunnan University, Kunming, China. [2]Department of Atmospheric Sciences, Yunnan University, Kunming, China. [3]Alfred Wegener Institute Helmholtz-Center for Polar and Marine Research, Bremerhaven, Germany. [4]Department of Physics and Electrical Engineering, University of Bremen, Bremen, Germany. [5]State Key Laboratory of Earth System Numerical Modeling and Application, Institute of Atmospheric Physics, Chinese Academy of Sciences, Beijing, China. ✉e-mail: wenqin.zhuo@ynu.edu.cn; yaoyao@tea.ac.cn

evolution of the large-scale atmospheric circulation in a more consistent way. This is the approach we are following here.

Event-based storyline simulations make it possible to explore potential climate scenarios for a specific circulation pattern with a high signal-to-noise ratio. This is in contrast to analyses based on free-running simulations which lack similarly close analogues in different climates due to internal variability. Moreover, the well-established probabilistic attribution approach[12], based on observational or free-running climate model data, does not distinguish between thermodynamic and dynamic drivers of change, with the latter being subject to considerable uncertainty because future dynamical changes remain debated[13]. Instead, an event-based storyline approach provides a clear picture of how climate change would affect specific extreme weather events through thermodynamic processes. The event-based storyline approach has been used to assess various extreme events in recent studies, including European heatwaves[10,14], marine heatwaves[15], droughts[16], Arctic moist and warm intrusions[17] and precipitation events[18,19]. However, how the thermodynamic component of climate change impacts specific cold extremes remains unexplored.

In the winter of 2020/21, three striking and impactful cold-air outbreaks successively burst across East Asia[20–23]. Each of these three cold events was more intense than the previous one, and the third event set a new low temperature record in most of the observation stations in northern China[20]. It has been suggested that the low Arctic sea ice extent in 2020 favored the occurrence of these three cold outbreaks through stratosphere-troposphere dynamic processes[21]. In addition, some external forcing such as SSTs have important synergistic effects[22,23]. Thus, the occurrence of successive cold air outbreaks may have been facilitated by preconditioned atmospheric dynamic settings. Blocking, a critical influence system of extreme weather[24–26], especially for cold events, can act as a bridge linking warm Arctic and cold continent[27]. However, as an important dynamic part of atmospheric internal variability, blocking is challenging to simulate due to its nonlinearity[28] and is usually underestimated in model simulations[29–32] On the other hand, the link between Arctic sea ice loss and the mid-latitude cold extreme weather is controversial and debated[33–37], due to limited understanding and apparent inconsistency between observations and model simulations[38]. Given the large uncertainty related to possible dynamical changes, it is worth exploring how the Arctic sea ice variation, under the same observational dynamic circulations in different climate backgrounds, would impact these cold extremes in a thermodynamic way. In event-based coupled storyline simulations, the circulation systems that lead to the observed cold events are retained to isolate the thermodynamic effect of climate change.

During the winter season, the state of the Arctic sea ice in future projections is closely linked with the level of anthropogenic forcing[39]. Even under low emissions SSP scenarios, Arctic amplification may continue to be enhanced by the inertia of the still-existing sea ice albedo feedback[40]. Therefore, in the context of continued global warming, the effects of Arctic amplification on cold extremes in winter over the mid-latitudes is expected to be an important factor. On the other hand, the variation of radiative forcing since pre-industrial periods, induced by increased aerosol emissions over East Asia[41,42], is also an important thermodynamic component of climate change. Therefore, in this work, we aim to examine three questions by employing storylines:

1. How would the three cold events in East Asia in 2020/21 winter have unfolded in a colder preindustrial era?
2. How would these cold events unfold in possible future (e.g., +2 °C or +4 °C relative to preindustrial) warmer climates?
3. What causes possible differences in the spatio-temporal patterns of the warming, and in how far do possible future changes resemble past changes?

Here the evolution of atmospheric circulation patterns leading to these three cold air outbreaks are reproduced in different climates via spectrally nudged experiments[10], thereby measuring the thermodynamic effects of climate change on the cold event.

Results

We use storyline simulations performed with the coupled climate model AWI-CM-1-1-MR[43]. These simulations, previously used to analyse heatwaves over land[10] and in the ocean[15], are used here to analyse the winter 2020/21 East Asian cold events. Previous studies have evaluated the performance of the AWI-CM-1-1-MR model, demonstrating reliable and robust performance within the CMIP6 ensemble[43,44]. In the storyline simulations, the observed free troposphere large-scale circulation (divergence and vorticity, 100-700 hPa) from ERA5 reanalysis data[45] is imposed to the model via spectral nudging in different background climates, following historical forcings followed by the Shared Socioeconomic Pathway scenario ssp370, which is a high greenhouse gas and high aerosol emission scenario. All other parameters (small scale, thermodynamics, ocean-ice-atmosphere interactions) are left to evolve freely according to the model's physics. Here, we present storylines of the winter 2020/21 cold events in four climate states: Preindustrial (PI), present-day (PD), and 2 °C and 4 °C warmer worlds, with each time slice comprising five ensemble members to sample remaining small-scale variability. See Methods for detailed information.

Assessment of nudged simulations in present-day climate over East Asia

Before we examine the cold events storylines in various climate states, we compare the nudged simulations in the present-day (PD) climate with the ERA5 data to establish the skill of the storyline system in capturing the essence of the observed extreme events (Fig. 1). We find similar temperature and circulation patterns in our simulations and ERA5. Note that, although we have nudged the dynamic part, here we are applying a relatively "soft" nudging where not all wavenumbers and levels are constrained and where the relaxation timescale is 24 hours, hence some discrepancies remain between the PD and ERA5 atmospheric circulation, reflected by differences in the 500hPa geopotential height fields (contour lines in Fig. 1). In the 2m-temperature anomaly fields, the warm anomalies over the northern Eurasian continent in the nudged experiments are weaker than in ERA5 (Fig. 1a–f), which may be related to a cold bias over the Arctic region in the nudged simulations which is also present in the free-runs[43].

From the timeseries of the 2m-temperature averaged over three regions (Fig. 1g), three cooling events can be identified over south China and middle East Asia, each marked by temperature drops of increasing intensity. These events align with a progressively strengthening 500-hPa blocking ridge and downstream trough (Fig.1f), reflecting stronger dynamical forcing in the later cases. Specifically, during the second and third cold case, Northeast Asia diverges in its temperature evolution from the patterns observed in the other two regions, indicating that it is located outside the core cooling regions during these two events, while still experiencing relatively low temperatures. Overall, despite some minor discrepancies with the reanalysed values, the temperature evolution over the three regions generally exhibits a consistent evolution with high correlation, especially during the periods of the three cold events. Therefore, the dynamic features and their associated response at the surface are overall well captured by the nudged simulations. The realistic representation of these extreme events justifies examining potential alterations of these three cold events due to thermodynamic effects of climate change with our methodology, by comparing how these events unfold in the different climate background states.

Storylines of East Asian cold events in winter 2020/21

We examine the temperature change of cold events in different climate states by comparing 4 °C warmer, 2 °C warmer and preindustrial (PI) climates with PD climate (Fig. 2). The degree of flow-dependence can be inferred by comparison with the corresponding differences derived from the free-running simulations (Fig. 2d, h, l). The 2m-temperature anomalies for each climate relative to PD is shown in Supplementary Fig. 1, and the amplitude of these changes compared to climatological changes (storylines minus free-runs) in Supplementary Fig. 2. Two prominent signals stand out. First, there is a strong warming over northeast Asia in the 4 °C-warmer climate state, especially on 30 Dec (Fig. 2b), which is weaker in the free-run

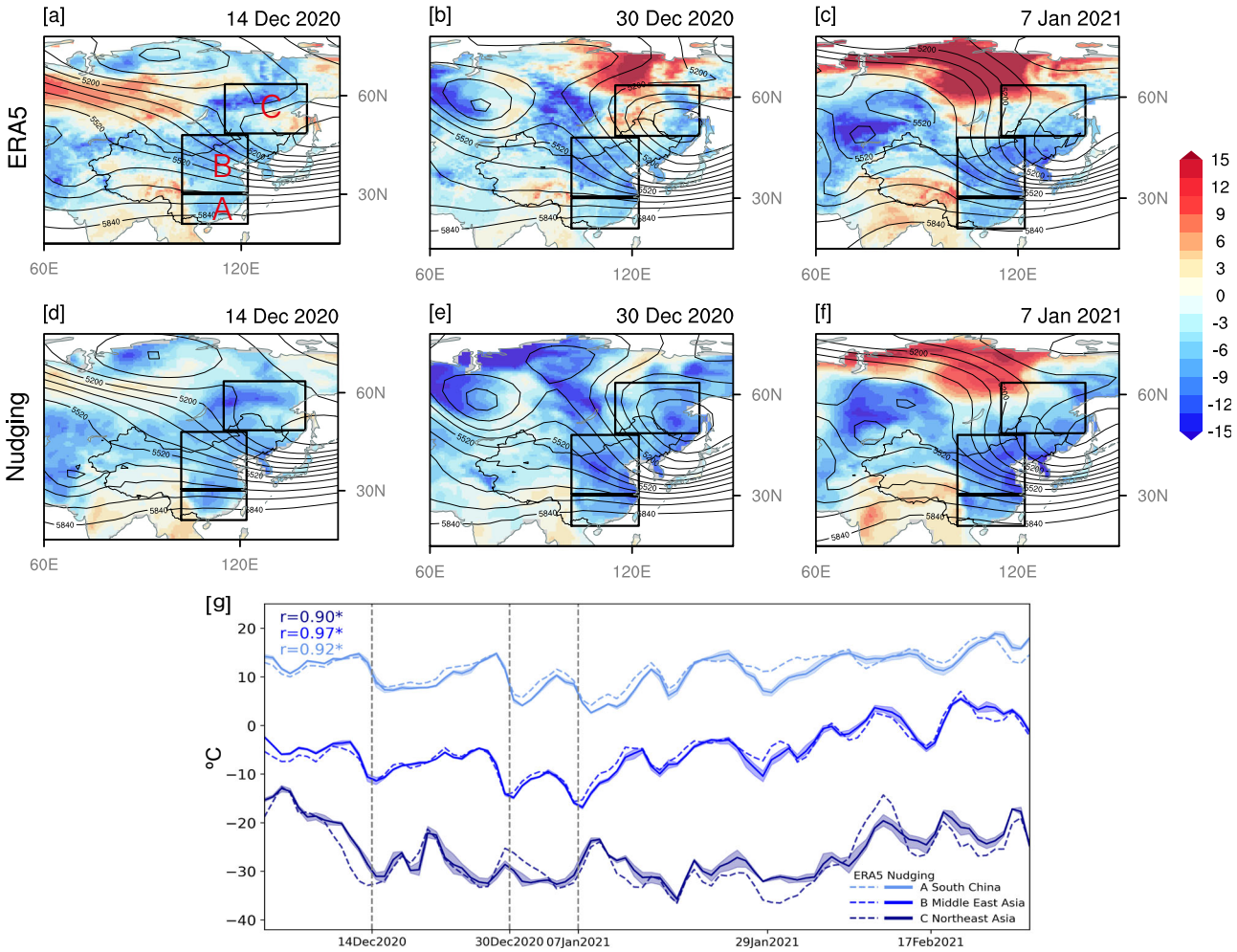

Fig. 1 | Comparison between ERA5 and AWI-CM1 present-day simulations with nudging. a–c ERA5 Daily mean 2 m air temperature anomalies (shading, °C) and 500-hPa geopotential height (contour, m) for three days corresponding to cold events in East Asia. **d–f** Same as in **a–c** but for present-day nudged simulations. The rectangles A, B, C denote South China, Middle East Asia and Northeast Asia, respectively. **g** Domain-averaged time series of 2m-temperature over the three regions during winter 2020/21. The shading for the nudged simulations shows the five-member ensemble spread. The correlation coefficients between ERA5 and the nudged simulations for each region are shown in the top left in corresponding colour, with * indicating significance at the 99% confidence level. Vertical dashed lines indicate the representative days of the three cold events depicted in **a–f**.

simulations (Fig. 2d), suggesting the presence of a flow-dependent signal specific to this cold extreme event (Supplementary Fig. 2b). Second, there is a weak but consistent cooling over South China between PI and PD (Fig. 2i, j, k), with additional cooling between PD and 2 °C for the first event (Fig. 2e). Third, over central East Asia, where the cold events have their peak, no further warming or cooling amplification appears when compared with free-run changes (Supplementary Fig. 2), meaning that the changes are in line with the average regional and seasonal climate warming patterns, that is flow-dependent climate change seems to play a minor role in this area. Based on these three features, we examine three regions more closely: northeast Asia (rectangle C), which is outside of the main region of the cold event but exhibits strong warming and flow-dependent amplification; middle East Asia (rectangle B) with changes close to the climatological regional changes; and South China (rectangle A) with weak cooling between PD and PI.

Consistent with the regional pattern (Fig. 2a–c), in a 4 °C warmer climate, the ensemble-mean temperature exhibits much stronger warming in Northeast Asia (Fig. 3a) compared to the more southern regions throughout December and January (Fig. 3b–c), with the timeseries closer to the free-runs warming. This phenomenon is consistent with a stronger influence of Arctic amplification in the North. Specifically, over Northeast Asia (Fig. 3a), on 30 Dec 2020 the 2m-temperature in PI, PD and 2 °C warmer climate remains well below the free-run climatology. But when it comes to the 4 °C warmer climate the anomaly is minimal. This is a consequence of a warming anomaly locally above 12 °C, with a high signal-to-noise ratio and amplified relative to the mean warming (Fig. 2d). Thus, this warming amplification beyond the climatological warming derived from the free-runs (Figs. S2b) in fact turns the second event, characterised by cold anomalies in the PI, PD and 2 °C warmer climates, into a situation with close to neutral anomalies in a 4 °C warmer climate (Fig. 3a) for the same large-scale circulation. This suggests that what used to be cold-air intrusions from the Arctic over Northeast Asia might bring rather milder conditions in a 4 °C warmer climate. In the third cold case, however, the warming is relatively weak and similar to the free-run (Fig. 2c, d, Supplementary Fig. 2c and Fig. 3).

Over Middle East Asia (rectangle B in Fig. 2), the storyline-based warming is similar to the climatological warming of the free-runs in all climate states, including for the three progressively intensifying temperature drops. Therefore, despite being a core region of cold events, Middle East Asia does not exhibit the strongly flow-dependent temperature amplification beyond the regional warming that we find for northeast Asia.

In contrast, over southern China (rectangle A in Fig. 2), where there is partly weak cooling instead of warming in PD climate compared to PI, the nudged simulations in PI, PD and 2 °C overlap for most of the time period (Fig. 3c), indicating that the cold anomalies (Fig. 2i–k) are not a temporal

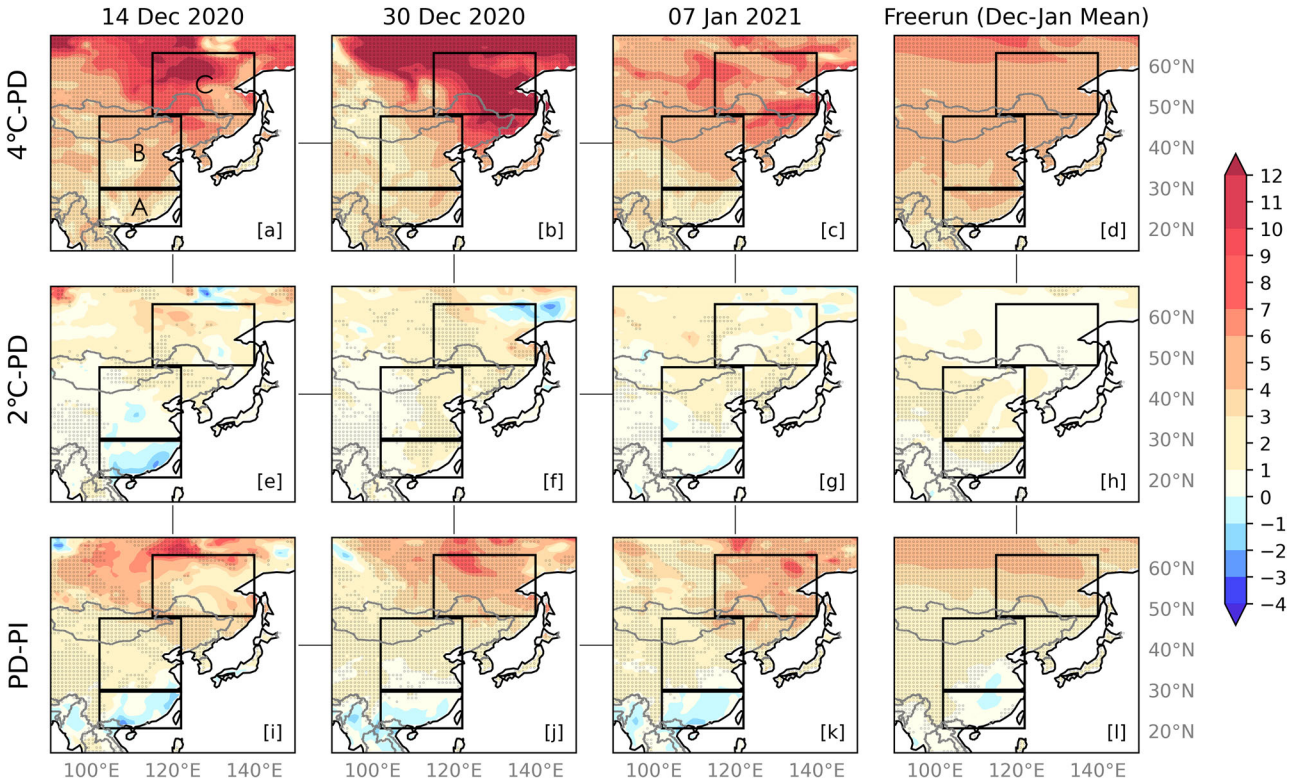

Fig. 2 | Changes in 2m-temperature (°C) of storylines scenarios in the three cold events. a–c +4 °C minus the present-day (PD), **e–g** +2 °C minus PD, and **i–k** PD minus preindustrial. The right panel (**d**, **h**, **l**) denotes the average of December and January of the smoothed free-run simulations. The rectangles A, B, C in (**a**) denote South China, Middle East Asia and Northeast Asia, respectively. Dotted regions denote non-overlapping ensembles, indicating a high signal-to-noise-ratio and statistical significance ($p < 0.008$).

exception. In fact, significant warming in South China in PD relative to PI climate is largely absent also in the free-runs (Fig. 2l). Comparing the storyline-based temperature change to the climatological change based on the free-runs reveals a weak warming dampening over South China in a 4 °C-warmer scenario (Supplementary Fig. 2a–c). As a consequence, even in a 4 °C-warmer climate, the temperature over south China during these events may remain below the PD climatology.

In the above analysis, we have shown the thermodynamic effects of climate changes on the winter 2020–2021 cold events, with a strong warming over Northeast Asia and a global warming dampening or even a slight cooling over South China. In the following, we examine processes driving these two contrasting responses.

The role of Arctic sea ice decline

The state of Arctic sea ice in the coupled nudged storyline simulations has been examined in a previous study[10]. Overall, the nudged experiments effectively capture the mean distribution of Arctic sea ice (Supplementary Fig. 3), although there are positive sea-ice concentration biases over parts of the ice-edge region that appear also in the free-running model[43]. Nevertheless, the simulations also broadly capture the observed internal variability of the sea-ice distribution[10].

According to the storyline simulations, dramatic sea ice loss occurs in a 4 °C-warmer climate (Fig. 4). The seasonal ice near the Eurasian continent in the Kara, Laptev, East Siberian and Chukchi Seas, and parts of the perennial ice are completely absent in early winter (Fig. 4a), which is a more pronounced reduction compared to the free-runs (Supplementary Fig. 4). The difference in sea ice reduction between nudged simulations and free-runs is closely related to the warming pattern under specific circulation (Supplementary Fig. 5). A strong warming by up to +20 °C occurs in regions that were formerly ice-covered but open ocean in a 4 °C warmer climate (Supplementary Fig. 5a–d). This is consistent with the key role of sea ice retreat in Arctic amplification. Many studies have pointed out that the Arctic is projected to become seasonally ice-free in summer in the near future[39,46]. In the late winter season, only the Barents Sea is expected to be completely ice-free by the end of the century under high emission scenarios[46], but the seasonal recovery of the ice in the Eurasian shelf seas occurs later as the warming proceeds, as simulated in the free-runs (Supplementary Fig. 4). Therefore, the prospect of occasionally ice-free conditions in the Arctic shelf seas in the winter season might have strong impacts on Eurasian cold events.

According to the air flows in the lower troposphere over the Arctic region, we can identify three distinct cold air paths during the considered events. In the first case, cold air is advected mainly from the west (Fig. 4a). These airflows partly come from a cyclonic system over northern Eurasia and partly originate from a ridge over the Ural Mountains. Since only a part of the air flow passes through the Arctic region, Northeast Asia exhibits relatively mild warming in this case (Fig. 2a). In the second case, a blocking ridge extends into the Arctic region and brings cold air mainly from the north (Fig. 4b), passing through the Laptev Sea area which is ice free in the 4 °C warmer climate. These airflows are due to the strong blocking that persisted for several days (Fig. S6). Meanwhile, the air masses mainly came from the ice-free Chukchi sea. The air-mass origin can explain the pronounced warming over Northeast Asia during the second event, as much milder cold air comes from regions of the Arctic Ocean (Supplementary Fig. 5) that used to be ice covered but may become ice-free in a 4 °C warmer climate. During the third case, which exhibits the weakest warming (Fig. 2c), air is advected mainly by northwesterly flow that originates partly in the Central Arctic (Fig. 4c). This event occurred later in winter, when most of the Arctic Ocean is frozen even in the 4 °C warmer climate, and the air does not pass regions with reduced sea-ice cover as much as during the second event. Therefore, the cold air transported by the airflow in the third case does

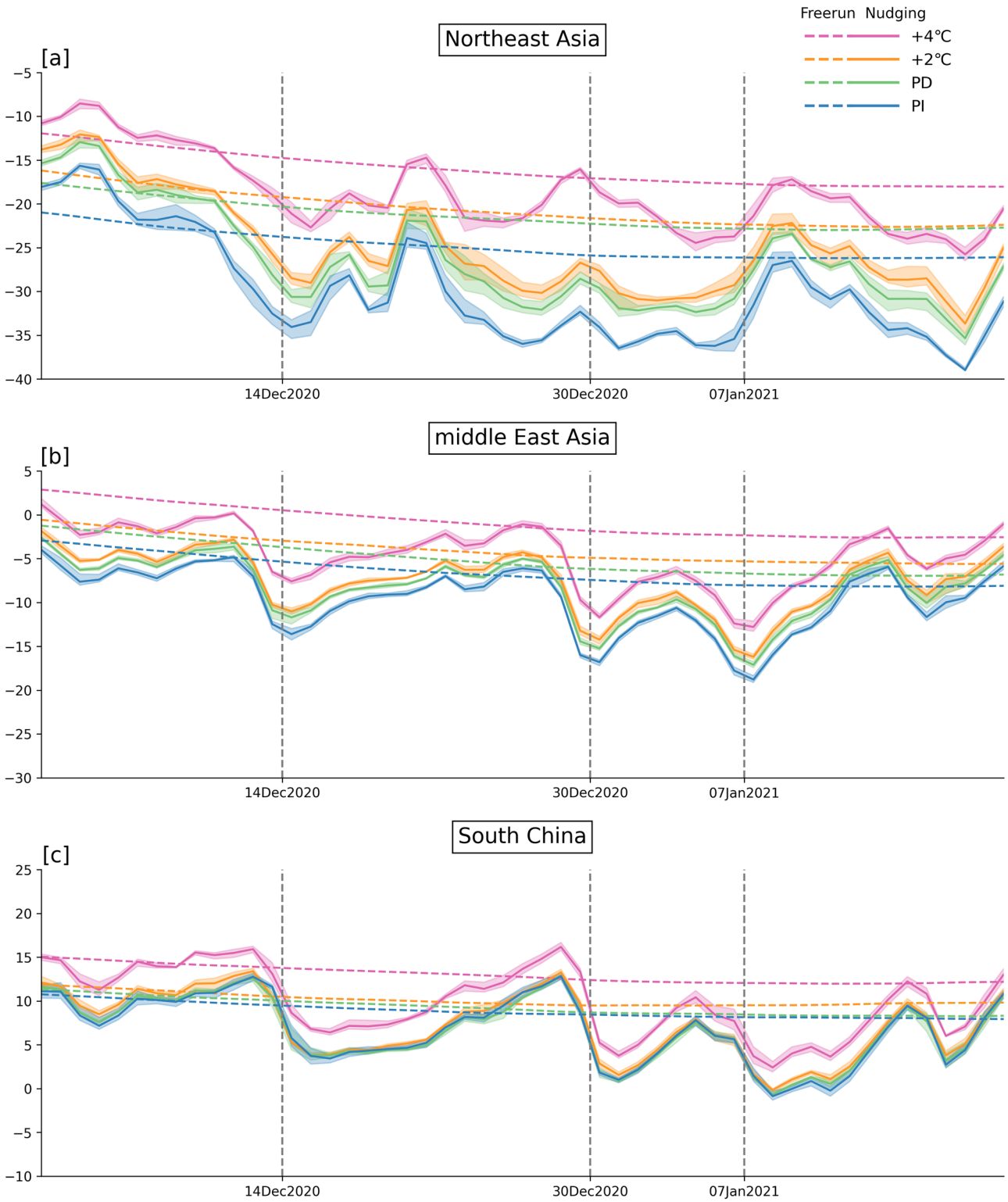

Fig. 3 | Evolution of 2m-temperature in three East Asian regions. 2m-temperature time series (°C) domain-averaged over (**a**) northeast Asia (48°N-63°N,115°E-140°E), (**b**) middle East Asia (30°N-48°N,102°E-122°E), and (**c**) South China (21°N-30°N,102°E-122°E), as outlined by the three rectangles in Fig. 2. Shading spans the range from the minimum to maximum values obtained from the five-member ensembles, and the solid (dashed) lines denote ensemble-mean values of the nudged storylines (free-runs). The vertical dashed lines denote the central days of the three cold events.

not warm up to the same extent as in the first and second cases, resulting in a less pronounced warming over northeast Asia. For the PD and 2 °C-warmer climates, however, the seasonal sea ice over high latitudes is almost unaffected (Supplementary Fig. 7), hence the warming amplification is not that clear during the three cold events (Fig. 2).

Shortwave radiative effects

While greenhouse gases primarily warm the surface through interaction with longwave radiation, transient aerosols and thermodynamic feedbacks in particular related to clouds can modify the surface response also through interaction with shortwave (solar) radiation. We find that the preindustrial

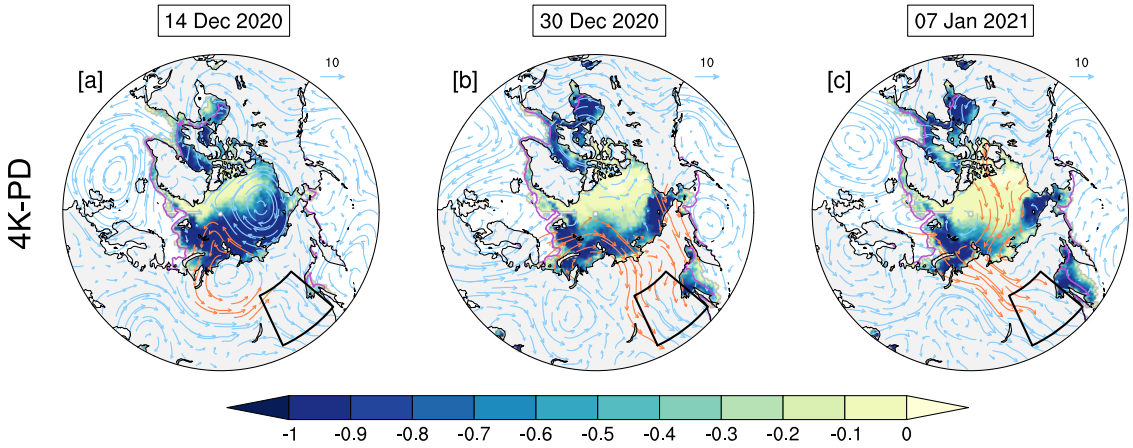

Fig. 4 | The role of reduced Arctic sea ice concentration. a–c Sea ice concentration difference fields between 4 °C and PD (shading) and 850-hPa wind vectors in the PD climate storyline simulations (vectors, m/s). Purple contours denote the climatological 15% sea ice concentration. The black box denotes the Northeast Asia region. Streamlines that have passed through the Arctic region and reached Northeast Asia are highlighted by orange vectors.

Fig. 5 | Effect of shortwave radiation on changes in the East Asian cold events. Time series of (**a**) downward net surface solar radiation (W/m²) and (**b**) total cloud cover over South China. Shading spans the range of the minimum/maximum values obtained from the five-member ensembles, and solid (dashed) lines denote the ensemble-mean from the nudged runs (free-runs). (**c–e**) Difference fields of surface downward solar radiation (W/m²) in clear-sky conditions between different climates, averaged between December and January. Black rectangles denote the South China region.

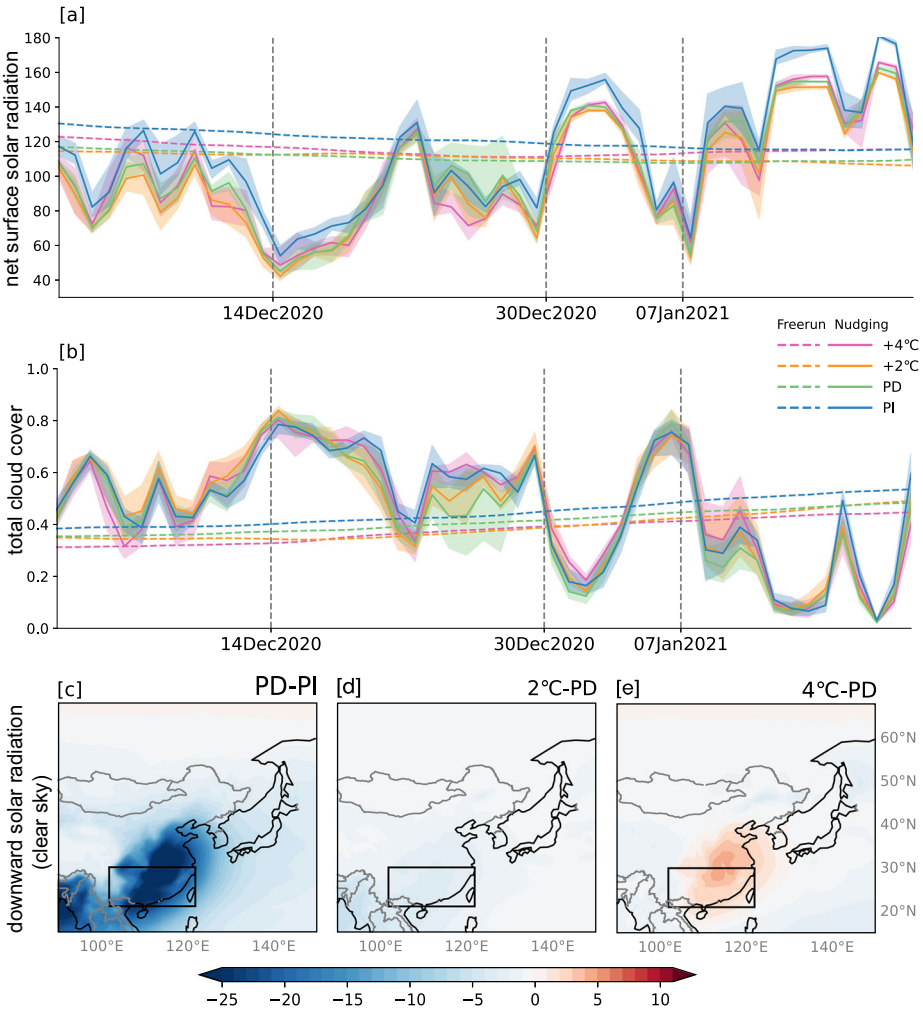

climate exhibits the highest downward net solar radiation over South China in both the nudged and the free-runs (Fig. 5a). In contrast, the 2 °C warmer and PD climates exhibit mostly lower net solar radiation, which is also noticeable in the free-runs (dashed lines in Fig. 5a). This reduced net solar radiation in PD and 2 °C warmer climates compared to PI periods coincides and therefore most likely drives the cooling over southern China.

Given that the surface net shortwave radiation is closely related to the cloud density, which can directly block the incoming solar radiation, we further examine the state of the total cloud cover (Fig. 5b). In the free-runs, warmer climates feature a reduction of the cloud cover (dashed lines in Fig. 5b); in the nudged simulations, however, except for the first case (14 Dec), there is no robust difference. Cloud reductions may thus explain some

shortwave-related warming in the free-runs, but the overall reduced surface shortwave heating does not seem to be related to clouds.

The downward solar radiation under clear-sky conditions (Fig. 5c–e, averaged for December and January) reveals a strong negative difference over the whole of South China in present-day compared to preindustrial conditions (Fig. 5c). The shortwave radiation continues to decrease towards a 2 °C warmer climate (Fig. 5d), and slightly recovers towards a 4 °C warmer climate (Fig. 5e), although remaining at lower values than in PI. The striking change of the clear-sky shortwave radiation in the PD compared to the PI climate suggests a strong direct aerosol effect. The spatial pattern of the decreasing downward solar radiation is consistent with the change pattern of aerosol optical depth over South Asia over the last decades[42,47–49]. Many studies have highlighted the non-negligible offsetting cooling effect of aerosols on greenhouse gas-induced global warming, especially over China[41,50]. It should be noted that the ssp370 scenario is a high aerosol emission scenario[51], where the emission of aerosols is expected to peak in the mid-21st century. In the 1980s, the aerosol-induced cooling effect could offset up to 80% of greenhouse gas-induced warming, whereas, according to ssp370 scenarios, this counterbalancing effect is expected to decrease to only 5-10% by the end of this century[50]. This is consistent with the positive changes in the downward solar radiation in the 4 °C warmer climate (Fig. 5e) relative to PD, when warming clearly dominates also in South China (Fig. 2a–d). Our results corroborate that the altered shortwave radiation balance between PD and PI climates induced by direct aerosol forcing has overcompensated the otherwise expected warming in this area, not only in general but also during the specific cold events 2020/21 considered here. This cooling effect might persist in a 2 °C warmer climate, but in a 4 °C warmer climate with reduced air pollution, cold events in winter over South China associated with circulation patterns like those in 2020/21 would experience a pronounced ubiquitous warming.

Discussion and conclusions

In this work, we develop storylines of three successive cold events in East Asia during the winter 2020/21 using nudged climate model simulations. This relatively new method allows us to quantify the thermodynamic effects of climate change on cold extremes, by fixing the dynamical component of the atmospheric circulation to the observed one through spectrally nudged experiments[10]. The storylines reveal how this series of cold events might have unfolded in a colder preindustrial era, and how the events might unfold in warmer climates undergoing 2 °C and 4 °C global-mean temperature rise relative to preindustrial conditions. Future alterations of East Asian cold extremes may have important socio-economic impacts given their relevance for agricultural production and human health.

We find two distinct and contrasting thermodynamic effects of climate change that influence cold events in East Asia. One is the prominent Arctic amplification effect in a 4 °C warmer climate, which could result in the strongest warming, locally exceeding +12 °C over Northeast Asia. This is related to reduced Arctic sea-ice cover in a 4 °C warmer climate. Consequently, when the northerly winds of a strong blocking ridge pass through a newly sea ice-free region, where the near-surface warming would exceed +20 °C, the previously very cold air entering East Asia would become much warmer. This leads to pronounced warming amplification in Northeast Asia and greatly diminishes the amplitude of the temperature drop during such an event. In the 2 °C warmer scenario, the seasonal sea ice and the associated lower temperatures in the relevant regions still tend to return earlier in winter, so the event-specific warming amplification in East Asia beyond the climate background warming is more modest. These results highlight the key influence of seasonal sea ice retreat and Arctic amplification on downstream land regions under strong warming scenarios.

Another thermodynamic effect explored here is associated with decreased net downward solar radiation over South Asia, resulting in a moderate cooling over South China in present-day climate compared to preindustrial for the considered events. This altered radiation balance is related to an increase in aerosol precursor emissions[42,48,49], which is projected to peak around the mid-21st century[50], a few years after the 2 °C-warmer climate is reached in AWI-CM with the ssp370 scenario. Therefore, this cooling effect may still largely compensate for the warming by greenhouse gases when similar cold events occur in a mid-century 2 °C-warmer climate, but would be much weaker than the warming by greenhouse gases in a 4 °C warmer climate. Given that the magnitude of aerosol forcing has been shown to be strongly model and scenario dependent[52], this aspect merits attention in future studies and model developments.

In conclusion, we have identified Northeast Asia as a region prone to a strong flow-dependent climate warming in winter. This is consistent with previous finding[11] which suggests that the accelerated warming of northerly winds caused by Arctic amplification is faster than that of the southerly winds, thereby decreasing the temperature variance in the cold season. Additionally, the weakening of the winter monsoon due to enhanced sea ice decline, neglected here by the prescribed atmospheric circulation, may further warm winters in East Asia[53]. We have quantified how mechanisms related to Arctic amplification and the associated temperature variance would affect cold extremes analogous to the winter 2020/2021 events. Among the three cold events, the second case, characterised by a northerly cold air path, experiences the strongest influence from Arctic warming. As a common and most influential cold wave path over East Asia, the northerly path is projected to continue causing future Arctic air intrusions[54]. The global warming level at which these air intrusions become much warmer is linked to the timing of the seasonal ice retreat near the Eurasian continent. The ice in these regions is dramatically reduced in a 4 °C-warmer climate, which leads to the warming cold air intruding into northeast Asia. This highlights the potential influence of seasonal ice variations on Eurasian extreme winter weather.

As demonstrated in previous studies[6,19], storylines do not show changes in the probability of cold events as in conventional model simulation studies, but rather help understanding the thermodynamic effects of climate change. Through the cold-event storylines examined here, we underscore the key role of Arctic amplification in a 4 °C-warmer climate in high-latitude regions, and aerosol-related radiation balance alterations under present-day and 2 °C-warmer climate states in lower latitudes under specific circulation conditions, at least in a high aerosol emission scenario. While the storyline approach does not account for potential dynamic responses of atmospheric circulation to climate change and their effects on extreme weather, our findings provide critical insights into how the thermodynamic effects of Arctic amplification and radiation budget change induced by aerosol emissions may influence extreme cold events through a storyline-based perspective.

Methods

Storyline simulations

We use simulation data based on AWI-CM-1-1-MR[43], which contributed to the Coupled Model Intercomparison Project Phase 6 (CMIP6)[55] and employs the ECHAM6.3.04p1 atmospheric model[56,57] coupled to the Finite Element Sea Ice–Ocean Model (FESOM) v.1.4[56]. We have extended the simulations from previous work[10] until 2021, which cover the East Asian cold events in 2020/21. The model's atmospheric circulation is constrained by nudging the vorticity and divergence based on the ERA5 dataset with a relaxation timescale of 24 h and a spectral truncation of 20 on zonal wavenumbers. Only vertical levels between 700-hPa and 100-hPa are nudged. We select four simulated climate conditions in which 2017–2021 dynamics are imposed: Preindustrial (PI) climate, branched from the 1851's of historical CMIP runs[58],present-day (PD) climate, branched from the Shared Socioeconomic Pathway scenario ssp370 runs[43] on 1st January 2017, and 2 °C and 4 °C warmer climates relative to preindustrial branched from the ssp370 scenario when these warming levels are reached (i.e., 1st January 2038 and 1st January 2093, respectively). Accordingly, the target time of 2020/21 cold events in the nudged simulation corresponds to the winter of 1854/55, 2020/21, 2041/42, 2096/97, when a stabilization has been reached after a certain spin-up period. For each different time slice we use five

ensemble members of nudged runs, branched from the five CMIP6 ensemble members available from AWI-CM-1-1-MR.

Free-run simulations

We use the ensemble mean of the five historical CMIP6 simulations and ssp370 scenario based on the model AWI-CM-1-1-MR, referred to as "free-run', for comparison with the nudged simulations[43,59,60]. The free-runs contain their own random realisation of internal variability without external dynamic forcing. Consistent with the nudged simulations, the target time of 2020/21 cold events in the free-run simulations corresponds to the winter of 1854/55, 2020/21, 2041/42, 2096/97, with a 31-day running mean to the multi-year climatology derived by averaging over the five available ensemble members. Previous studies have systematically evaluated the performance of CMIP6 models and identified AWI-CM-1-1-MR as a relatively realistic model[44,61]. The model climatology is not strongly affected by the nudging[10,15], enabling direct comparisons between the nudged simulations and the free-runs.

Reanalysis data

We use daily 2m-temperature and 500-hPa geopotential height from ERA5 reanalysis data to conduct results comparison between present-day climate in nudging experiment and observational dataset.

Anomalies and climatology

The 2m-temperature anomalies of the nudged data in all scenarios are determined by subtracting the climatology for the period 1985–2014. The climatology is calculated as the ensemble mean of the five historical free run simulation. To minimise sampling effects, we apply a 31-day running mean to the multi-year climatology derived by averaging over the five available ensemble members. The same time-filtering way is used for the ERA5-based climatology required to calculate ERA5-based anomalies. When comparing the different climate periods, the free-run climatology is calculated using an 11-yr centered moving window average from the free-runs.

Storyline, event-specific change and study regions

The storyline of cold events denotes the changes of a given parameter in winter 2020/21 at 4 °C, 2 °C warmer world and PI climate compared to PD climate. An event-specific change refers to a warming or cooling feature observed when baseline global warming extent, i.e., the climatology background, is subtracted from the storyline warming. Warming amplification indicates a greater warming in storyline compared to the climatological mean[10,15]. Accordingly, we divided the study regions into three areas according to regional event-specific change characteristics: Northeast Asia (48 °N-63 °N,115 °E-140 °E), which shows strongest warming amplification in a 4 °C-warmer climate (Fig. 2a–c); middle East Asia (30 °N-48 °N,102 °E-122 °E), similar to the climatological warming of the free-runs results (Fig. 2e–g); and South China (21°N-30 °N,102 °E-122 °E), which has weak cooling in PD and 2 °C-warmer climate compared to PI world (Fig. 2i–k).

High signal-to-noise-ratio

When analysing the storyline simulations, we quantify climate change signals by comparing each climate state (e.g., PI or 4 °C-warmer climate) to the PD baseline. For a given grid point, we define statistically robust signals as regions where the five-member ensemble ranges of two compared climates show no overlap. 'No overlap' means, for example, that the minimum value across all members in a 4 °C-warmer climate is greater than the maximum value across all members of the PD climate. This strict non-overlap criterion (equivalent to a two-sided Wilcoxon test p-value of 0.008) identifies areas with high signal-to-noise ratios, indicating event-specific amplification where warming signals consistently dominate internal variability across all ensemble members[15].

Data availability

The data of the nudged experiments are stored in the supercomputer Levante at DKRZ and are available online (Zenodo: https://doi.org/10.5281/zenodo.13984784). Data from the AWI-CM-1-1MR free-runs are available from the Earth System Grid Federation (ESGF) data nodes (e.g., https://esgf-data.dkrz.de/search/cmip6-dkrz/). ERA5 reanalysis data used in this study can be accessed from the Copernicus Climate Data Store (C3S).

Code availability

The source codes for the analysis of this study are available from the corresponding author upon reasonable request.

Received: 21 November 2024; Accepted: 31 March 2025;
Published online: 06 May 2025

References

1. Chylek, P. et al. Annual Mean Arctic Amplification 1970–2020: Observed and Simulated by CMIP6 Climate Models. *Geophys Res Lett.* **49**, e2022GL099371 (2022).
2. Rantanen, M. et al. The Arctic has warmed nearly four times faster than the globe since 1979. *Commun. Earth Environ.* **3**, 1–10 (2022).
3. Johnson, N. C., Xie, S. P., Kosaka, Y. & Li, X. Increasing occurrence of cold and warm extremes during the recent global warming slowdown. *Nat. Commun.* **9**, 4–6 (2018).
4. Van Oldenborgh, G. J., Haarsma, R., De Vries, H. & Allen, M. R. Cold extremes in North America vs. mild weather in Europe: The winter of 2013-14 in the context of a warming world. *Bull. Am. Meteorol Soc*. **96,** 707–714 (2015).
5. Mori, M., Watanabe, M., Shiogama, H., Inoue, J. & Kimoto, M. Robust Arctic sea-ice influence on the frequent Eurasian cold winters in past decades. *Nat. Geosci.* **7**, 869–873 (2014).
6. Shepherd, T. G. et al. Storylines: an alternative approach to representing uncertainty in physical aspects of climate change. *Clim. Change* **151**, 555–571 (2018).
7. Schär, C., Frei, C., Lüthi, D. & Davies, H. C. Surrogate climate-change scenarios for regional climate models. *Geophys Res Lett.* **23**, 669–672 (1996).
8. Brogli, R., Heim, C., Mensch, J., Sorland, S. L. & Schar, C. The pseudo-global-warming (PGW) approach: Methodology, software package PGW4ERA5 v1.1, validation, and sensitivity analyses. *Geosci. Model Dev.* **16**, 907–926 (2023).
9. Vries, H., de, Lenderink, G., Meijgaard, E., van, Ulft, B. van & Rooy, W. de. Western Europe's extreme July 2019 heatwave in a warmer world. *Environ. Res.: Clim.* **3**, 035005 (2024).
10. Sánchez Benítez, A., Goessling, H., Pithan, F., Semmler, T. & Jung, T. The July 2019 European heatwave in a warmer climate: Storyline scenarios with a coupled model using spectral nudging. *J. Clim.* 1–51 (2022).
11. Screen, J. A. Arctic amplification decreases temperature variance in northern mid- to high-latitudes. *Nat. Clim. Chang* **4**, 577–582 (2014).
12. Philip, S. et al. A protocol for probabilistic extreme event attribution analyses. *Adv. Stat. Climatol. Meteorol. Oceanogr.* **6**, 177–203 (2020).
13. Shepherd, T. G. A Common Framework for Approaches to Extreme Event Attribution. *Curr. Clim. Change Rep.* **2**, 28–38 (2016).
14. Wehrli, K., Hauser, M. & Seneviratne, S. I. Storylines of the 2018 Northern Hemisphere heatwave at pre-industrial and higher global warming levels. *Earth Syst. Dyn.* **11**, 855–873 (2020).
15. Athanase, M., Sánchez-Benítez, A., Goessling, H. F., Pithan, F. & Jung, T. Projected amplification of summer marine heatwaves in a warming Northeast Pacific Ocean. *Commun. Earth Environ.* **5**, 1–12 (2024).
16. van Garderen, L. & Mindlin, J. A storyline attribution of the 2011/2012 drought in Southeastern South America. *Weather* **77**, 212–218 (2022).

17. Pithan, F. et al. Nudging allows direct evaluation of coupled climate models with in-situ observations: A case study from the MOSAiC expedition. *EGUsphere* **1**, 23 (2022).
18. Gessner, C., Fischer, E. M., Beyerle, U. & Knutti, R. Developing Low-Likelihood Climate Storylines for Extreme Precipitation Over Central Europe. *Earths Future* **11**, e2023EF003628 (2023).
19. Athanase, M., Sánchez-Benítez, A., Monfort, E., Jung, T. & Goessling, H. F. How climate change intensified storm Boris' extreme rainfall, revealed by near-real-time storylines. *Commun. Earth Environ. 2024 5:1* **5**, 1–5 (2024).
20. Yao, Y., Zhang, W., Luo, D., Zhong, L. & Pei, L. Seasonal Cumulative Effect of Ural Blocking Episodes on the Frequent Cold events in China during the Early Winter of 2020/21. *Adv. Atmos. Sci.* **31**, 243–251 (2021).
21. Dai, G., Li, C., Han, Z., Luo, D. & Yao, Y. The Nature and Predictability of the East Asian Extreme Cold Events of 2020/21. *Adv. Atmos. Sci.* (2021).
22. Yu, Y. et al. An Isentropic Mass Circulation View on the Extreme Cold Events in the 2020/21 Winter. *Adv. Atmos. Sci.* **39**, 643–657 (2022).
23. Zhang, X. et al. Extreme Cold Events from East Asia to North America in Winter 2020/21: Comparisons, Causes, and Future Implications. *Adv. Atmos. Sci.* **39**, 553–565 (2022).
24. Pfahl, S. & Wernli, H. Quantifying the relevance of atmospheric blocking for co-located temperature extremes in the Northern Hemisphere on (sub-)daily time scales. *Geophys Res Lett.* **39**, 12807 (2012).
25. Nakamura, N. & Huang, C. S. Y. Atmospheric blocking as a traffic jam in the jet stream. *Science (1979)* **361**, 42–47 (2018).
26. Kautz, L.-A. et al. Atmospheric blocking and weather extremes over the Euro-Atlantic sector – a review. *Weather Clim. Dyn.* **3**, 305–336 (2022).
27. Luo, D. et al. Weakened Potential Vorticity Barrier Linked to Recent Winter Arctic Sea Ice Loss and Midlatitude Cold Extremes. *J. Clim.* **32**, 4235–4261 (2019).
28. Luo, D., Chen, X., Dai, A. & Simmonds, I. Changes in Atmospheric Blocking Circulations Linked with Winter Arctic Warming: A New Perspective. *J. Clim.* **31**, 7661–7678 (2018).
29. Barnes, E. A. & Hartmann, D. L. Influence of eddy-driven jet latitude on North Atlantic jet persistence and blocking frequency in CMIP3 integrations. *Geophys. Res. Lett.* **37**, GL045700 (2010).
30. Scaife, A. A., Woollings, T., Knight, J., Martin, G. & Hinton, T. Atmospheric blocking and mean biases in climate models. *J. Clim.* **23**, 6143–6152 (2010).
31. Brunner, L., Schaller, N., Anstey, J., Sillmann, J. & Steiner, A. K. Dependence of Present and Future European Temperature Extremes on the Location of Atmospheric Blocking. *Geophys. Res. Lett*. **45**, 6311–6320 (2018).
32. Tibaldi, S. & Molteni, F. On the operational predictability of blocking. *Tellus, Ser. A* **42**, 343–365 (1990).
33. Blackport, R., Sigmond, M. & Screen, J. A. Models and observations agree on fewer and milder midlatitude cold extremes even over recent decades of rapid Arctic warming. *Sci. Adv.* **10**, eadp1346 (2024).
34. Cohen, J., Francis, J. A. & Pfeiffer, K. Anomalous Arctic warming linked with severe winter weather in Northern Hemisphere continents. *Commun. Earth Environ. 2024 5:1* **5**, 1–13 (2024).
35. Cohen, J., Agel, L., Barlow, M., Garfinkel, C. I. & White, I. Arctic change reduces risk of cold extremes: Response. *Science (1979)* **375**, 729–730 (2022).
36. Hong, Y. et al. From peak to plummet: impending decline of the warm Arctic-cold continents phenomenon. *NPJ Clim. Atmos. Sci.* **7**, 1–5 (2024).
37. Wu, B., Li, Z., Francis, J. A. & Ding, S. A recent weakening of winter temperature association between Arctic and Asia. *Environ. Res. Lett.* **17**, 034030 (2022).
38. Cohen, J., Zhang, X., Francis, J. & Al, E. Divergent consensuses on Arctic amplification influence on midlatitude severe winter weather. *Nat. Clim. Chang* **28**, 7917–7932 (2019).
39. Notz, D. & Community, S. Arctic Sea Ice in CMIP6. *Geophys Res Lett.* **47**, e2019GL086749 (2020).
40. Ono, J., Watanabe, M., Komuro, Y., Tatebe, H. & Abe, M. Enhanced Arctic warming amplification revealed in a low-emission scenario. *Commun. Earth Environ.* **3**, 1–9 (2022).
41. Persad, G. G. & Caldeira, K. Divergent global-scale temperature effects from identical aerosols emitted in different regions. *Nat. Commun. 2018 9:1* **9**, 1–9 (2018).
42. Freychet, N., Tett, S. F. B., Bollasina, M., Wang, K. C. & Hegerl, G. C. The Local Aerosol Emission Effect on Surface Shortwave Radiation and Temperatures. *J. Adv. Model Earth Syst.* **11**, 806–817 (2019).
43. Semmler, T. et al. Simulations for CMIP6 With the AWI Climate Model AWI-CM-1-1. *J. Adv. Model Earth Syst.* **12**, e2019MS002009 (2020).
44. Merrifield, A. L., Brunner, L., Lorenz, R., Humphrey, V. & Knutti, R. Climate model Selection by Independence, Performance, and Spread (ClimSIPS v1.0.1) for regional applications. *Geosci. Model Dev.* **16**, 4715–4747 (2023).
45. Hersbach, H. et al. The ERA5 global reanalysis. *Q. J. R. Meteorol. Soc.* **146**, 1999–2049 (2020).
46. Kim, Y. H., Min, S. K., Gillett, N. P., Notz, D. & Malinina, E. Observationally-constrained projections of an ice-free Arctic even under a low emission scenario. *Nat. Commun. 2023 14:1* **14**, 1–8 (2023).
47. He, J. Y., Xie, B., Zhang, H. & Yu, X. C. Impacts of greenhouse gases and anthropogenic aerosols changes on surface air temperature in East Asia under different post-pandemic period emission scenarios. *Adv. Clim. Change Res.* **13**, 884–895 (2022).
48. Fiedler, S. et al. Historical Changes and Reasons for Model Differences in Anthropogenic Aerosol Forcing in CMIP6. *Geophys. Res. Lett.* **50**, e2023GL104848 (2023).
49. Liu, S. et al. Understanding of Aerosol–Climate Interactions in China: Aerosol Impacts on Solar Radiation, Temperature, Cloud, and Precipitation and Its Changes Under Future Climate and Emission Scenarios. *Curr. Pollut. Rep.* 36–51 (2019).
50. Bauer, S. E. et al. The Turning Point of the Aerosol Era. *J. Adv. Model Earth Syst.* **14**, 1–17 (2022).
51. Gidden, M. J. et al. Global emissions pathways under different socioeconomic scenarios for use in CMIP6: A dataset of harmonized emissions trajectories through the end of the century. *Geosci. Model Dev.* **12**, 1443–1475 (2019).
52. Schumacher, D. L. et al. Exacerbated summer European warming not captured by climate models neglecting long-term aerosol changes. *Commun. Earth Environ. 2024 5:1* **5**, 1–14 (2024).
53. Dong, J. et al. Arctic sea ice loss warmed the temperate East Asian winter in the mid-Holocene. *Commun. Earth Environ. 2024 5:1* **5**, 1–10 (2024).
54. Yang, X., Zeng, G., Zhang, G. & Li, C. Linkage between interannual variation of winter cold surge over East Asia and autumn sea ice over the Barents Sea. *Theor. Appl Climatol.* **144**, 339–351 (2021).
55. Eyring, V. et al. Overview of the Coupled Model Intercomparison Project Phase 6 (CMIP6) experimental design and organization. *Geosci. Model Dev.* **9**, 1937–1958 (2016).
56. Stevens, B. et al. Atmospheric component of the MPI-M Earth System Model: ECHAM6. *J. Adv. Model Earth Syst.* **5**, 146–172 (2013).
57. Wang, Q. et al. The Finite Element Sea Ice-Ocean Model (FESOM) v.1.4: Formulation of an ocean general circulation model. *Geosci. Model Dev.* **7**, 663–693 (2014).
58. Semmler, T. et al. AWI AWI-CM1.1MR model output prepared for CMIP6 CMIP historical. *Earth System Grid Federation*, accessed 12 January 2021 (2018).
59. Sidorenko, D. et al. Towards multi-resolution global climate modeling with ECHAM6–FESOM. Part I: model formulation and mean climate. *Clim. Dyn.* **44**, 757–780 (2015).

60. Rackow, T. et al. Towards multi-resolution global climate modeling with ECHAM6-FESOM. Part II: climate variability. *Clim. Dyn.* **50**, 2369–2394 (2018).
61. Lee, J. et al. Systematic and objective evaluation of Earth system models: PCMDI Metrics Package (PMP) version 3. *Geosci. Model Dev.* **17**, 3919–3948 (2024).

Acknowledgements

This work was supported by the Helmholtz Research Field Earth & Environment for the Innovation Pool Project SCENIC. All simulations were performed at the German Climate Computing Center (DKRZ) using ESM Tools[58] and resources from the ba1264 project. W.Q.Z. acknowledges the financial support by China Scholarship Council and China Postdoctoral Science Foundation (2024M762757). Y.Y. acknowledges the financial support by the National Natural Science Foundation of China (Grant 42375061).

Author contributions

W.Q.Z. plotted all figures and wrote the initial manuscript. A.S.-B. conducted the model experiments and processed the data. H.F.G., A.S.-B., T. J. contributed to the experiment design and results analysis. M.A. and Y.Y. contributed to the improvement of the manuscript. All authors contributed to the discussions and reviewed the manuscript.

Funding

Open Access funding enabled and organized by Projekt DEAL.

Competing interests

The authors declare no competing interests.

Additional information

Supplementary information The online version contains supplementary material available at https://doi.org/10.1038/s41612-025-01031-x.

Correspondence and requests for materials should be addressed to Wenqin Zhuo or Yao Yao.